Journal of The Electrochemical Society, **158** (4) A371-A378 (2011)
0013-4651/2011/158(4)/A371/8/$28.00 © The Electrochemical Society

Implementing Realistic Geometry and Measured Diffusion Coefficients into Single Particle Electrode Modeling Based on Experiments with Single $LiMn_2O_4$ Spinel Particles

M. D. Chung,[a,*] J. H. Seo,[a] X. C. Zhang,[a,] and A. M. Sastry[a,b,c,**,z]**

[a]*Department of Mechanical Engineering,* [b]*Department of Biomedical Engineering, and* [c]*Department of Materials Science and Engineering, University of Michigan, Ann Arbor, Michigan 48109-2125, USA*

Realistic geometry and diffusion coefficients were measured from a single particle $LiMn_2O_4$ electrode and implemented into a three-dimensional multiphysics simulation of a single particle, in order to demonstrate a novel approach to electrode material study. Dispersed particles were used, and electrochemical techniques and atomic force microscopy were performed on isolated single particles. Diffusion coefficients measured from both cyclic voltammetry and the potentiostatic intermittent titration technique ranged between 3.2×10^{-12} and 1.2×10^{-11} cm^2/s, which was similar to values measured from thin film $LiMn_2O_4$ electrodes. The trend of diffusivity change over potential (versus lithium counter electrode) was similar to those observed from both composite cells and thin film electrodes. The measured diffusion coefficients were then used in simulation of discharge of the irregular particle, by importing the particle morphology into a finite element simulation, in order to simulate intercalation-induced stress generation. Simulation results showed a higher maximum stress generation due to altering diffusivity around the peak current potentials and high local stress concentration on the sharply indented surface area, suggesting that particle irregularities are important in studying both electrochemical performance and local failure mechanisms in cathode materials.
 [DOI: 10.1149/1.3549161]

Manuscript submitted May 10, 2010; revised manuscript received December 14, 2010. Published February 17, 2011.

Recent efforts in large-scale vehicle electrification have intensified interest in selecting, characterizing, and validating the performance of cathode materials. Among present candidates, the $Li_xMn_2O_4$ spinel ($0 < x < 1$) system is of high interest because of its high voltage, low cost, and low toxicity. It has been widely studied experimentally and by electrode modeling and simulations.[1–3] Key results from these studies, including simulations of reaction fluxes and intercalation-induced stresses, were found to be highly dependent upon material properties, especially Li ionic diffusivity.

Though convenient, assumptions of spherical or ellipsoidal electrodes in previous battery modeling must be reevaluated in light of the fact that irregular but realistic electrode shapes of active materials affect electrochemical behavior. To improve electrode modeling, and eventually to predict battery cell performance and failure with higher fidelity, it is essential to accurately characterize these parameters as well as materials diffusivity. Conversely, for cases in which reduced order models can be plausibly used, it is critical to understand the limits of such analyses.[1,2]

The diffusion coefficient of $Li_xMn_2O_4$ spinel ($0 < x < 1$) has been measured as a function of Li-ion concentration in a number of studies. Mainly, composite cells [Table I (Refs. 4–8)] and thin films [Table II (Refs. 9–13)] have been used to experimentally determine diffusion coefficients by cyclic voltammetry (CV), electrochemical impedance spectroscopy (EIS), and potentiostatic intermittent titration technique (PITT). As shown in Tables I and II, there are substantial disagreements in reported values, with discrepancies of up to 3 orders of magnitude.

While disagreements of up to 2 orders of magnitudes among composite electrodes and thin films may be attributed to the additives in composite electrodes such as binders and conducting agents, differences in electrode structures, from the crystalline microstructure to the cluster macrostructure, also play an important role. Dokko et al.,[14,15] for example, showed that crystalline grain and particle size significantly affect diffusion coefficients, as measured from microprobe-cycled single crystal and single particle electrodes. Thus, $Li_xMn_2O_4$ cathode materials of any type have different micro- to macrostructures and so have different diffusion properties depending on their manufacturing and fabrication process and conditioning. More realistic simulation requires a new experimental approach to measure diffusion coefficients from known electrodes as a form of isolated particles, involving only the active cathode materials in the electrochemical process, and also to identify realistic electrode geometry.

Table I. Review of diffusion coefficients of Li-ion in composite electrodes $Li_xMn_2O_4$.

D (cm^2/s)	x	Technique	Ref.
0.5 to 1.5×10^{-9}	0 and $0.5 \le x \le 1.0$	PITT	4
0.66 to 1.4×10^{-10}	$0.1 \le x \le 0.8$	PITT	5
4.89×10^{-9}	$0.2 \le x \le 0.8$	CV	6
5×10^{-10}	$0 \le x \le 1.0$	CV	7
2.2×10^{-9}	$0.17 \le x \le 1.0$	CV	8

Our research aims to implement realistic parameters from experimental samples into simulations of the electrochemical reaction within single particle cathodes of known composition and structure. We use the same experimental samples to validate our simulation models by measuring electrochemical and/or mechanical responses, such as strains. The overall research sequence including present and ongoing work is shown in Fig. 1. In this study, we have the following specific objectives:

(1) To demonstrate an experimental method for diffusivity measurements on dispersed particle electrodes via CV and PITT.
(2) To generate three-dimensional (3D) particle model geometries by processing surface scan images obtained from atomic force microscopy (AFM).
(3) To determine the effect of all key factors on stresses in cathodes, including diffusivity (processing type and geometry) and particle morphology.

Table II. Review of diffusion coefficients of Li-ion in thin film $Li_xMn_2O_4$.

D (cm^2/s)	SOC	Technique	Deposition	Ref.
3.5×10^{-11}	—	CV	PLD	9
6.1×10^{-12}	4.0 V	PITT	ESD	10
0.3 to 5.5×10^{-11}	3.9–4.3 V	PITT	ESD	11
0.47 to 5.96×10^{-12}	$x = 1.4$	CV, PITT	Sol-gel	12
0.46 to 1.04×10^{-11}	$x = 0.5$	CV	PLD	13
10^{-12} to 10^{-10}	3.85–4.3 V	EIS		
0.19 to 8×10^{-11}	3.85–4.5 V	PITT		

* Electrochemical Society Student Member.
** Electrochemical Society Active Member.
z E- mail: amsastry@umich.edu

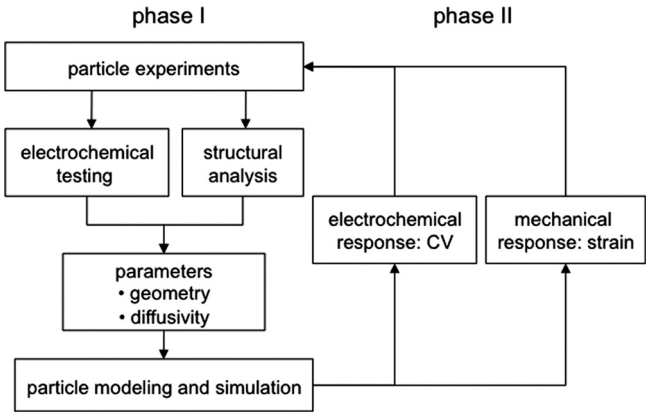

Figure 1. A schematic diagram of research sequence to bridge experiments to modeling (phase I, present work) and to validate the model (phase II).

Methods

Experimental.—Dispersions of particle electrodes of $Li_xMn_2O_4$ were prepared on gold foil current-collecting substrates. We adapted methods described by Totir et al.[7] and Clemencon et al.[16] to fabricate pure cathode particle electrodes. Electrodes prepared by Totir et al.[7] were lithium transition metal oxide particles closely packed on Au foils, while the electrode samples prepared by Clemencon et al.[16] were dispersed $LiCoO_2$ particles made for AFM measurement. In this study, similar efforts were made to isolate the $LiMn_2O_4$ particles, but with a higher degree of dispersion by using ultrasonication.

We prepared the electrode samples by (1) mixing raw $LiMn_2O_4$ powder (99.5%, Alfa Aesar) into acetone suspension with a ratio of 1 wt %, (2) dispersing the $LiMn_2O_4$ powder in an acetone suspension by an ultrasonic wave for 60 min, (3) depositing the $LiMn_2O_4$ particles onto a gold foil (99.99%, Aldrich) from a drop of suspension, and (4) gradually pressing the particles against a counter gold foil up to 20 kpsi using a preprogrammed material compression tester (Instron). Once the counter gold piece was carefully removed, the particle-topped electrodes were examined by scanning electron microscopy (SEM) for larger scale observation, and AFM for microscale characterization. AFM (MultiMode coupled with a NanoScope controller, Veeco) on single particle electrodes was used to reconstruct the 3D particle geometry with MATLAB and HYPERMESH for image processing and meshing.

The sample used for electrochemical experiments was dispersed particles of $LiMn_2O_4$ on the gold foil. The gold foil was the current collector, and a number of particles were cycled as the active cathode material. The active surface area was calculated by first measuring how much area was occupied by the particles in a unit area through SEM (~13%), then by estimating the spherical surface area for a 3×3 mm sample size. For the electrochemical measurements, these dispersed particle samples were assembled in a Swagelok cell containing electrolyte of 1 M $LiPF_6$ in ethylene carbonate (EC) and diethyl carbonate (DEC) (1:1 in volume, Merck) with lithium foil counter electrodes, all inside an Ar-filled glovebox (<1 ppm O_2 and H_2O). The assembled cells were permitted to dwell for about an hour and then measured for open-circuit potential (OCP) before galvanostatic cycling at a rate of C/50 between the OCP and 4.5 V using a VMP3 potentiostat/galvanostat (Bio-Logic). Cyclic voltammograms were collected between 3.5 and 4.5 V at a sweep rate from 0.05 to 1.0 mV/s. For the PITT measurements, a potential step of 10 mV was applied between 3.85 and 4.30 V while the current transition was measured until the absolute current value reached below 10 nA at the equilibrium state. All electrochemical tests were conducted at room temperature (298 K).

Analytical for diffusivity measurement.—The peak currents measured from CV were used to calculate the diffusion coefficients as follows. The relationship was derived from a diffusion equation describing spherical electrodes[17] as

$$\frac{\partial C_O(r,t)}{\partial t} = D_O\left[\frac{\partial^2 C_O(r,t)}{\partial r^2} + \frac{2}{r}\frac{\partial C_O(r,t)}{\partial r}\right] \quad [1]$$

where C_o is the concentration of the diffusion component (lithium ions), D_o is the diffusion coefficient of Li ion, r is the distance from the center of the electrode, and t is the time. This equation can be solved using the initial condition that the concentration of lithium ions is uniformly given by the bulk concentration at the beginning of the electrochemical reaction and two additional boundary conditions. One boundary condition is obtained from Nernst equation with potential sweep given as

$$\frac{C_O}{C_R} = \frac{f_R}{f_O}\exp\left[\frac{nF}{RT}(E_i - E^0)\right]\exp\left[\frac{nF}{RT}vt\right] \quad [2]$$

where f_R and f_o are activity coefficients of substances, n is the charge number, E_i and E^0 are the initial and the standard potentials, v is the potential scan rate, F is Faraday constant, R is the gas constant, and T is absolute temperature. Another boundary condition is the equilibrium condition at the electrode surface, that is

$$D_O\frac{\partial C_O(r_o,t)}{\partial r} + D_R\frac{\partial C_R(r_o,t)}{\partial r} = 0 \quad [3]$$

A solution for this diffusion Eq. 1 and boundary conditions, Eqs. 2 and 3, was provided by Frankenthal and Shain[18] for the peak of the current–voltage curve at room temperature (25°C) as

$$i_p = (8.81 \times 10^5)n^{3/2}AD_O{}^{1/2}C_O{}^0v^{1/2}\partial C_O(r_o,t)/C_O^0 \quad [4]$$

where i_p is the peak current in amperes, A is the electrode surface area in square centimeter, D_o is the diffusion coefficient in square centimeter per second, C_O^0 is the bulk concentration in mole per cubic centimeter, and v is the potential scan rate in volts per second. The extrapolated value of the term $\partial C_O(r_o,t)/C_O^0$ was obtained from the experimental data in Ref. 18. The peak current in spherical electrodes for Li-ion diffusion can be estimated to be

$$i_p = (2.74 \times 10^5)n^{3/2}AD_O{}^{1/2}C_O^0v^{1/2} \quad [5]$$

The current response to a step potential from PITT can be expressed by a Cottrell equation for a short time region as

$$i(t) = nFA(C_S - C_O^0)(D_{app}/\pi t)^{1/2} \quad [6]$$

and by the finite diffusion approximation for a longer time region as

$$i(t) = \frac{2nFA(C_S - C_O^0)D_{app}}{r}\exp\left(-\frac{\pi^2 D_{app}t}{r^2}\right) \quad [7]$$

where r is the radius of a spherical particle, C_s the concentration of Li ion at the surface, C_O^0 the bulk Li-ion concentration inside a particle, and D_{app} the apparent diffusion coefficient. In the long time approximation in Eq. 7, the diffusion coefficient can be evaluated from the slope of a linear plot of ln $i(t)$ vs t without information about concentration when the radius of the particle is known.

Single particle simulation.—A single particle $LiMn_2O_4$ electrode model was used to simulate the Li-ion diffusion and the intercalation-induced stress, following prior work,[1,2] but including new parameters of realistic particle geometry and concentration-dependent diffusion coefficients. In our previous modeling, the Li-ion diffusion, expressed as the diffusion flux, was given by[1]

$$J = -D\left(\nabla c - \frac{\Omega c}{RT}\nabla\sigma_h\right) \quad [8]$$

where c is the Li-ion concentration, Ω is the partial molar volume of lithium, σ_h is the hydrostatic stress, D is the diffusion coefficient, R is the general gas constant, and T is temperature. From this equation, the Li-ion species mass conservation equation was obtained as

$$\frac{\partial c}{\partial t} + \nabla \cdot \left[-D\left(\nabla c - \frac{\Omega c}{RT} \nabla \sigma_h \right) \right] = 0 \quad [9]$$

At the particle boundary, the diffusion flux can be expressed by the current density i_n as

$$J = -D\left(\nabla c - \frac{\Omega c}{RT} \nabla \sigma_h \right) = \frac{i_n}{F} \quad [10]$$

where F is Faraday constant.

The Li-ion diffusion kinetics is determined via the Butler–Volmer equation as

$$J = \frac{i_n}{F} = \frac{i_0}{F}\left(\exp\left[\frac{(1-\beta)F}{RT}\eta \right] - \exp\left[-\frac{\beta F}{RT}\eta \right] \right) \quad [11]$$

where i_0 is exchange current density, η is surface overpotential, and β is symmetry factor. The exchange current density is given by

$$i_0 = Fk(c_l)^{1-\beta}(c_\theta)^{1-\beta}(c_s)^{\beta} \quad [12]$$

where c_l is the Li-ion concentration in the electrolyte, c_s is the Li-ion concentration on the surface of the solid electrode, c_θ is the concentration of available vacant sites on the surface ready for lithium intercalation ($c_{max} - c_s$), and k is a reaction rate constant.[2] Input parameters for these diffusion equations are given in Table III. The intercalation-induced stress model was derived by thermal stress analogy to the constitutive equation between stress and strain[1] as

$$\varepsilon_{ij} = \frac{1}{E}\left[(1+\nu)\sigma_{ij} - \nu\sigma_{kk}\delta_{ij} \right] + \frac{\tilde{c}\Omega}{3}\delta_{ij} \quad [13]$$

where ε_{ij} are strain components, σ_{ij} are stress components, E is Young modulus, v is Poisson ratio, $\tilde{c} = c - c_0$ is the Li-ion concentration change, and Ω is the partial molar volume of lithium. A Young modulus $E = 10$ GPa and a partial molar volume $\Omega = 3.497 \times 10^{-6}$ m^3/mol were assumed. Eqs. 9 and 13 are coupled through the Li-ion concentration and the stress components.

Results and Discussion

Electrode characterization.—The dispersed $LiMn_2O_4$ particles embedded on the gold foil were imaged via SEM (Fig. 2). The average size of cathode particles was 4 μm; higher magnification images revealed the particle to have flat, crystalline surfaces, as shown in Fig. 2b. In Fig. 3, SEM images of individual $LiMn_2O_4$ particles on a carbon mesh show the grain boundaries and provide the grain size. The size of the unit crystal was observed to be around 1 μm; 4–5 crystals form a particle with about 2 μm radius was used for the diffusion length. The size of the unit crystal was 20–40% of the particle size but certainly within the same order of magnitude. Three-dimensional surface geometry of the particle was obtained via AFM

Table III. Parameters for the single particle electrode simulation.

Parameter (symbol)	Value
Li-ion concentration in the electrolyte (c_l)	1000 mol/m^3 (Ref. 13)
Maximum Li-ion concentration (c_{max})	2.37×10^4 mol/m^3 (Ref. 2)
Reaction constant (k)	1.9×10^{-9} m$^{5/2}$s^{-1}mol$^{-1/2}$ (Ref. 2)
Potential cycling rate (v)	0.5 mV/s
Diffusion coefficient (D as function of c)	$0.3–1.2 \times 10^{-11}$ cm^2/s (Fig. 7)

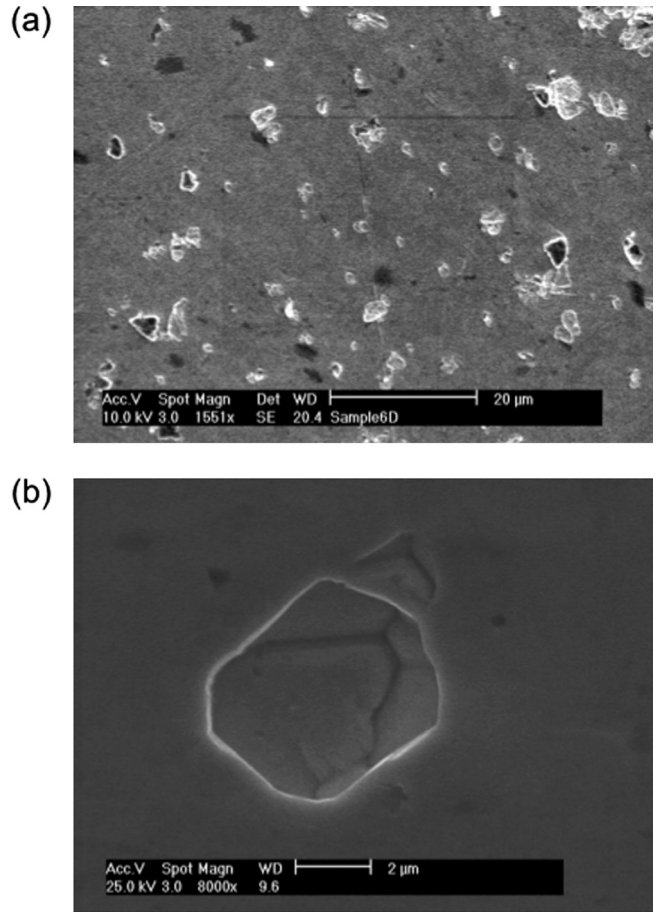

Figure 2. SEM images of (a) $Li_xMn_2O_4$ dispersed particle electrode and (b) single particle with a crystal surface parallel to a gold substrate.

(Fig. 4). The surface area of the dispersed particle electrode was estimated from a number of SEM photographs to be 0.0237 cm^2 for 3×3 mm sample substrate. The sectional analysis of the particle surface profile confirmed that the particles were securely connected to the current collecting gold substrate as shown in Fig. 4; this was also confirmed by good galvanostatic and cyclic voltammetry behaviors of the electrode.

Electrochemical behaviors.—$LiMn_2O_4$ particle electrodes were cycled at a constant current rate of C/50 (~10 μA/cm^2) between the initial OCP to 4.5 V, against lithium foil counter electrodes for the initial formation cycle. The galvanostatic voltage profile showed well-defined potential plateaus at 3.94 and 4.13 V. This suggests that the removal of a Li ion takes place in two steps around 4 V versus lithium, which is in good agreement with previous galvanostatic measurements of $Li_xMn_2O_4$ ($0 < x < 1$) composite[4,6] and thin film electrodes.[13] The two-phase (de)insertion process of Li ion at the tetrahedral sites in the spinel structure was also confirmed by the two well-defined peaks from cyclic voltammograms at lower scan rates (Fig. 5). The first anodic peak potential was 4.01 V, and the second anodic peak potential was 4.14 V. Cathodic peak potentials were 3.99 and 4.11 V versus a lithium counter electrode (Fig. 5b). The relative heights of the two peaks in Fig. 6 are consistent with those reported for CV measurements of composite cells[5,19] and microvoltammetry of single particle electrodes,[15,20] while the reverse trend has been reported in the case of $LiMn_2O_4$ thin film fabricated with pulsed laser deposition (PLD).[9] Because the electrodes used in this study were pure $LiMn_2O_4$ spinel particles without carbon and binder (as in the case of single particle studies in Refs.15 and 20), our CV results can provide a good comparison and

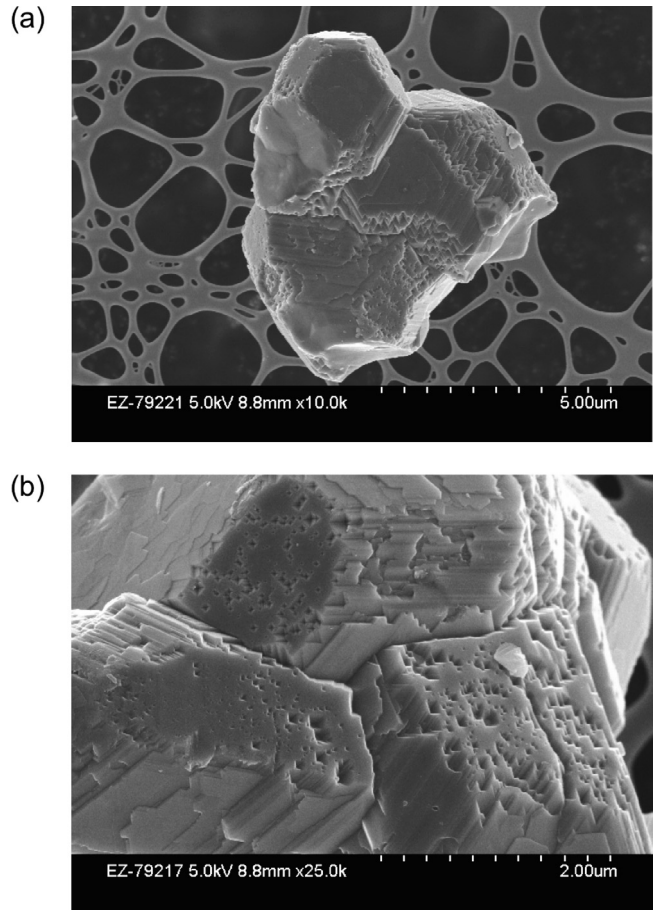

Figure 3. SEM images of (a) a $LiMn_2O_4$ spinel particle and (b) crystal grains and grain boundary

answer a question raised in the thin film study[9]; the reverse trend of relative peak heights from the thin film electrodes might originate from characteristics of the thin film microstructures and its fabrication condition.

Diffusivity measurements.—Both CV and PITT were used for estimating chemical diffusion coefficients for Li-ion intercalation within the particle $Li_xMn_2O_4$ electrodes. The trends of peak current versus potential scan rate from the cyclic voltammograms are shown in Fig. 6. The peak current values of both Li ion (de)insertion processes are linearly dependent on the square root of the scan rate ($v^{1/2}$), as expected for diffusion-controlled reactions as derived in Eq. 5. With a given charge number, the bulk concentration of Li ion in $LiMn_2O_4$ (given as $C_O^0 = 0.02378$ mol/cm^3 from the theoretical density of spinel), and the estimated electrode surface area from SEM/AFM images, we can calculate the Li-ion diffusion coefficients from the slope of peak current versus the square root of the scan rate ($v^{1/2}$) in Fig. 6. The results are summarized in Table IV. The diffusion coefficients for four different peaks are very similar, ranging between 1.70×10^{-11} and 2.94×10^{-11} cm^2/s; the oxidation process shows slightly higher diffusion coefficients than reduction, which is in good agreement with previous measurements of Li-ion diffusivity using CV.[6,13]

PITT (Ref. 21) was also used to determine the chemical diffusion coefficients of Li ions in the $Li_xMn_2O_4$ spinel particles. As discussed in a previous diffusion study,[22] the use of Eq. 7 can provide more reliable diffusion coefficients than Eq. 6, because the approximation of Eq. 7 is strongly influenced by the surface roughness of the particle. The Cottrell equation usually depends on the surface condition as this semi-infinite diffusion model is applicable only for

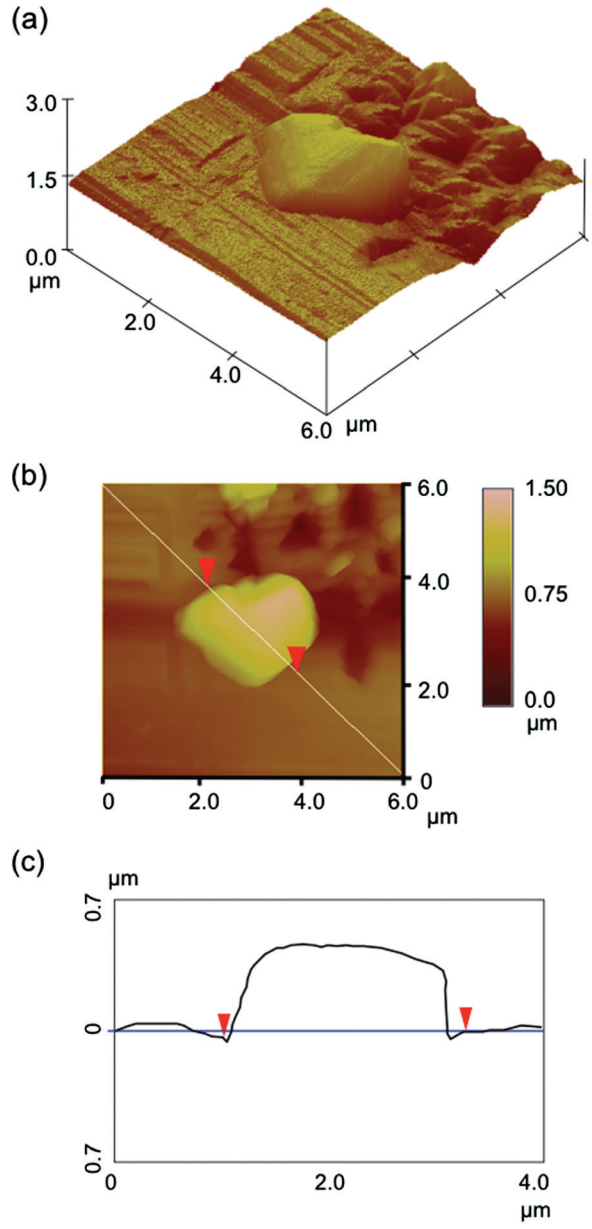

Figure 4. (Color online) AFM images of $Li_xMn_2O_4$ single particle by tapping mode on a scan size of 6×6 μmml: (a) 3D image, (b) 2D profile of surface height, and (c) section analysis on a cross section line indicated by red arrows. The tuning frequency of the tapping probe was 277.15 kHz, and the scan rate was 0.5 Hz.

a short time range when the thickness of the diffusion layer is generated at the interface. Additionally, the current is often nonlinear with respect to time for short timescales ($t \ll r^2/D_{app}$). For most of the potential steps between 3.85 and 4.30 V, nonlinear current responses were observed from the short time range while consistent linear behaviors of the current were shown at the long time regions from the Cottrell plots. Thus, in this study, we used Eq. 7, the long time approximation of the potential stepped current response for the measurement of Li-ion diffusion coefficients.

The resulting diffusion coefficients determined for the $Li_xMn_2O_4$ ($0 < x < 0.85$) when the electrode potential was between 3.85 and 4.30 V (vs Li/Li+) are shown in Fig. 7 for both the Li-ion insertion and extraction processes. For both (de)insertion processes, the diffusion coefficients from PITT show strong dependency on the Li-ion concentration within the potential range (3.85–4.30 V). The trends of the diffusion coefficients shown in Fig. 7 are similar to those

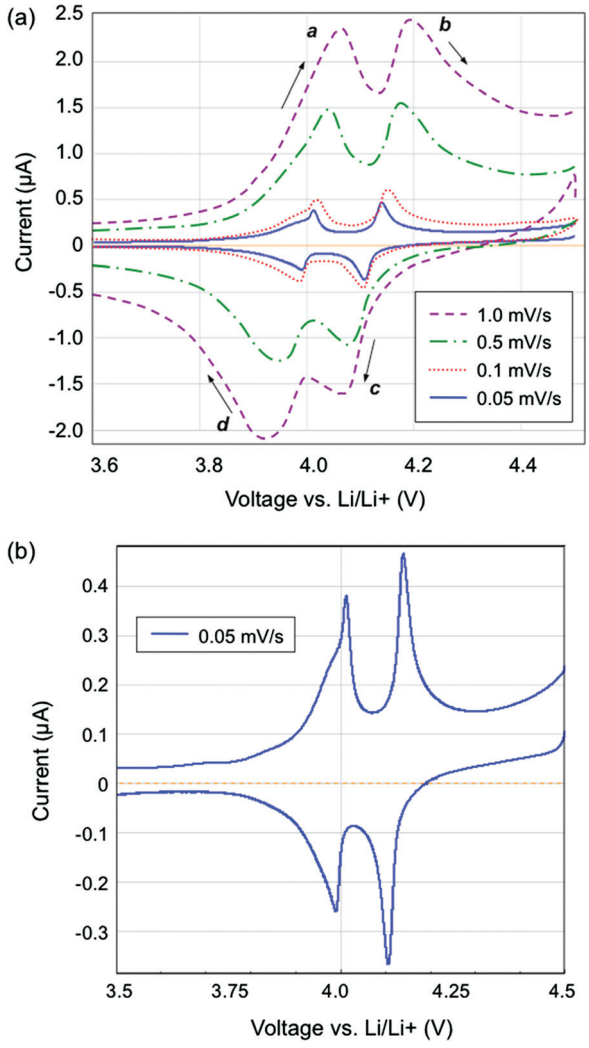

Figure 5. (Color online) Cyclic voltammetry of a $Li_xMn_2O_4$ dispersed particle electrode at scan rates from 0.01 to 1.0 mV/s. The current peaks are labeled by (a) and (b) for oxidation (charging) and (c) and (d) for reduction (discharging) peaks, respectively.

Table IV. Diffusion coefficients of Li-ion in dispersed particle $Li_xMn_2O_4$ electrode calculated from CV.

	D_o (cm^2/s)
Oxidation (anodic reaction)	
$LiMn_2O_4 \rightarrow Li_{0.5}Mn_2O_4$ (peak a)	2.94×10^{-11}
$Li_{0.5}Mn_2O_4 \rightarrow \lambda$-$MnO_2$ (peak b)	2.83×10^{-11}
Reduction (cathodic reaction)	
λ-$MnO_2 \rightarrow Li_{0.5}Mn_2O_4$ (peak c)	1.70×10^{-11}
$Li_{0.5}Mn_2O_4 \rightarrow LiMn_2O_4$ (peak d)	2.40×10^{-11}

reported by other researchers who studied either powder-based composite cells or thin film electrodes,[11–13,15] but the values ranging between 3.0×10^{-12} and 1.2×10^{-11} cm^2/s (3.95–4.15 V) are closer to the case of thin film measurements than the results from the composite cells as summarized in Fig. 8. In this figure, the diffusivities are compared with respect to the electrode geometry (composite, thin film, and single or dispersed particle) and by measurement techniques (CV, PITT, and EIS). Diffusion measurement by CV results in higher diffusion coefficients than by PITT or EIS in any form of electrode, while the difference was smaller in our experiment. Thin films in the literature and particle electrodes in the present study show similar diffusion coefficients ranging from 10^{-12} to 10^{-11} cm^2/s, while bulk or composite cell experiments produced higher diffusion coefficients by 2 orders of magnitude. This disparity indicates that the higher diffusion coefficients measured in composite cathodes might be due to the additive materials, especially conductive additives as they can alter the conducting path of the electrode and mislead the current reading. The diffusion properties from thin film electrodes, on the other hand, greatly depend on the film deposition methods; for example, the thin films fabricated by PLD show different diffusion properties from those produced by electrostatic deposition (ESD). Even in one fabrication method, specific process conditions can change the film properties (i.e., density, crystallinity, and surface morphology) and its diffusivity. Thus, for the purpose of measuring accurate diffusion properties for the porous cathode materials, the particle-based experiment proposed in this study can serve as a good method, as it is unaffected by either the additive materials or the film fabrication technique. The realistic diffusion properties from pure cathodes are important parameters to

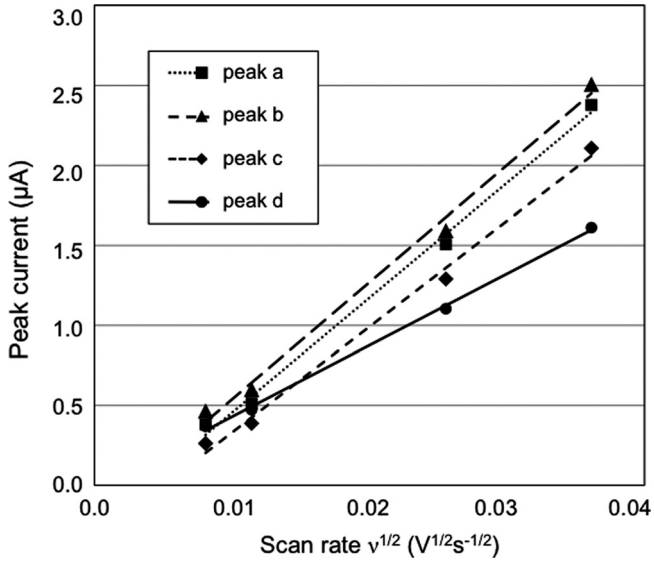

Figure 6. Peak current vs square root of scan rate ($v^{1/2}$) with peaks a, b, c, and d as labeled in cyclic voltammograms in Fig. 5.

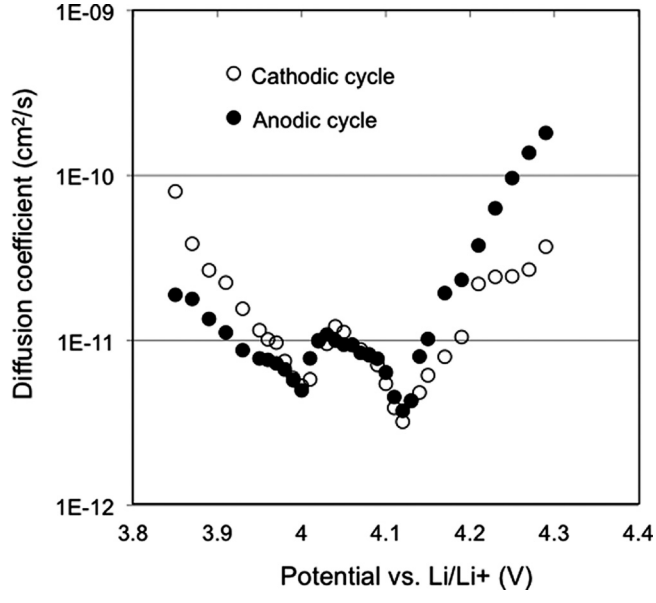

Figure 7. Diffusion coefficients of Li-ion as a function of electrode potentials vs Li/Li+ obtained from PITT for anodic and cathodic reactions.

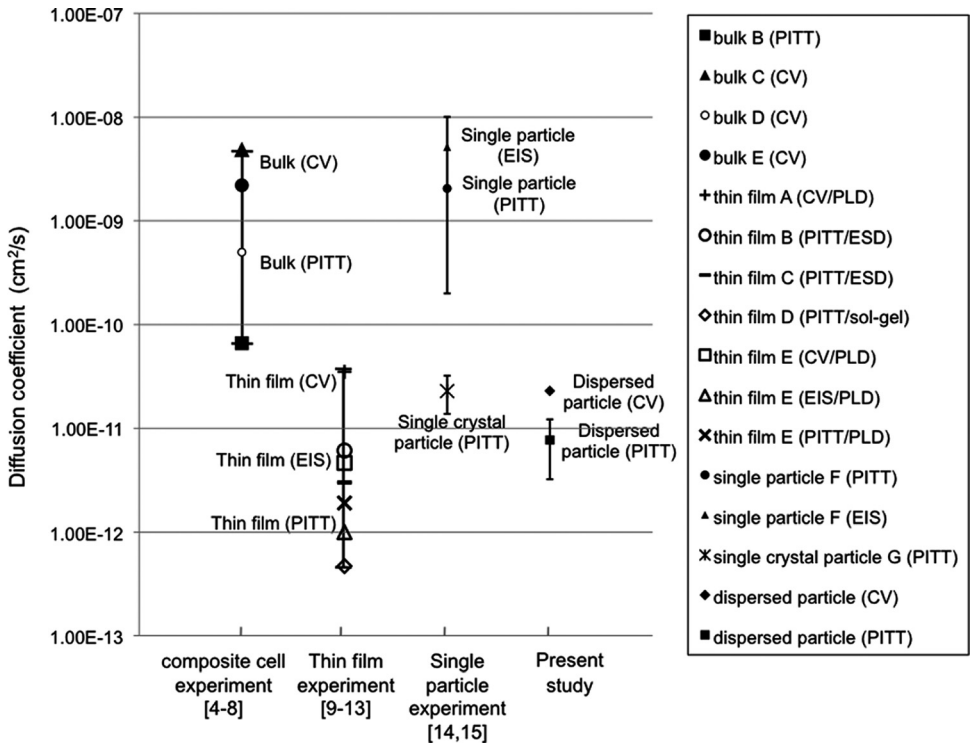

Figure 8. Comparison of diffusion coefficients.

accurately predict the mechanical and electrochemical behaviors of the materials in conventional Li-ion batteries using powder-based cathodes; as demonstrated in the following section, the difference in the diffusion coefficients and the consideration of their trend over the voltage range significantly affect the stress generation within the $LiMn_2O_4$ cathode particle. Figure 8 also provides comparison of our study to the single particle experiments by microvoltammetry technique, which measured diffusion properties of $LiMn_2O_4$ single crystal[14] and polycrystalline particle of the same material.[15] There is 2–3 orders difference in the apparent diffusion coefficients measured from our dispersed particle experiment and those from single $LiMn_2O_4$ polycrystalline particles in the literature. Meanwhile, $LiMn_2O_4$ single crystal showed lower diffusion coefficients of 10^{-10} to 10^{-11} cm^2/s, which is similar to our results. This difference (and similarity to single crystal case) seems to be caused by the crystalline size and Li-ion transfer within the grain boundaries. The crystalline grains from earlier single particle study[15] appear to be 200–300 nm, which is 3–5 times smaller than the unit crystal size of present study. Smaller crystallites form much denser grain boundaries and denser polycrystalline particles. This may explain the 2–3 orders difference in the apparent diffusion coefficients in the two studies.

Single particle simulation.—In former studies,[1,2] particle geometries were assumed to be either spheres or ellipsoids, and the stress localization due to subparticle structures such as crystalline grains and grain boundaries were not considered in the stress calculation. Irregular particle geometries as shown in SEM (Figs. 2 and 3) and AFM (Fig. 4) images can result in localized stress distribution and concentration, which may cause a local particle fracture and an eventual electrode failure. A 3D particle model was reconstructed based on AFM scan data from a dispersed $LiMn_2O_4$ particle sample and then imported into the simulation tool COMSOL Multiphysics. Once the clouds of surface points are identified, then the developed HYPERMESH scripts automatically generate the surface. It takes a couple of hours to generate the surface geometry of particles in a quad-core workstation of 2.66 GHz central processing unit (CPU). The initial condition for electrode concentration was applied based on the initial OCP. The boundary conditions were applied for Li-ion flux determined by Eq. 11 and free traction force on the top surface between a particle electrode and electrolyte, and also for zero Li-ion flux and point-fixed displacement on the bottom surface between a particle electrode and gold substrate. Theoretically, it is possible to extend this study to the composite electrode. This study can be easily extended with identified material phases, even though the composite solid electrode includes multiphase materials (e.g., binders, conductive additives, and active materials).

The simulation results for intercalation-induced stresses are shown in Fig. 9 at two different surface points: one on a smooth flat surface (point A), and the other on a sharply indented boundary, which is the most probable region of grain boundaries (point B). The concentration dependent diffusion coefficients measured by PITT as shown in Fig. 7 were used for this simulation. The von Mises stress curves over the potential range shown in Fig. 9a follow a pattern similar to the CV curve from the same cathode particle cell (Fig. 5). However, the maximum von Mises stress of 110 MPa measured from point B is 30% higher than the maximum stress from point A. Li-ion intercalation-induced stress is concentrated at the sharply indented boundaries on the particle surface geometry, as illustrated in Fig. 9b. Stress distribution on the particle surface shows that (i) larger stress occurs around the center of the flat particle surface where the diffusion path is shorter and the concentration change is larger and (ii) the irregular particle geometry leads to local stress concentration, especially through the sharply indented boundaries. Therefore, microstructure or detailed particle geometry should be considered to predict the highest stress generation during the Li-ion intercalation, which may eventually be responsible for the cell failure.

Another aspect of our simulation is the consideration of actual diffusion coefficients measured from the single $LiMn_2O_4$ particle electrode. As discussed earlier, diffusivity from the particle experiment was 1–2 orders of magnitude lower than that from composite cell experiments in the literature. Furthermore, the diffusion coefficient significantly changes over the potential range of our interest (between 3.95 and 4.15 V), as the Li ion (de)intercalates through

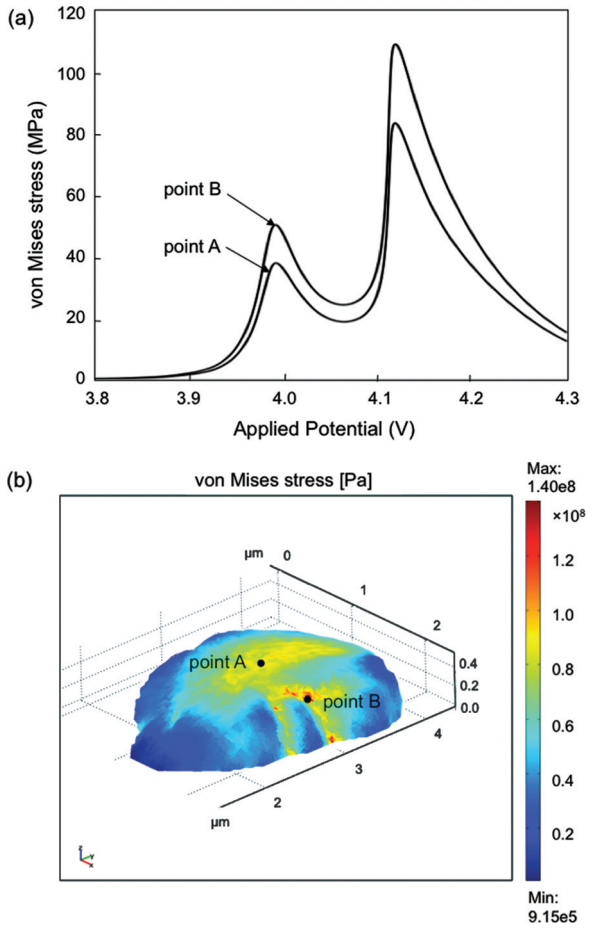

Figure 9. (Color online) Simulation with realistic particle geometry and concentration dependent diffusion coefficients with scan rate $v = 0.5$mV/s: (a) von Mises stresses on the top surface (point A) and at the sharply indented boundary (point B) and (b) von Mises stress distribution on the particle surface.

$Li_xMn_2O_4$ cathode and alternates its concentration. To compare the effect of diffusion coefficients on the stress generation within an electrode particle, simulations were run using three different diffusivities. Figure 10 shows stress generation with (i) the minimum value, 3.0×10^{-12} cm^2/s from our PITT measurement, (ii) diffusion coefficients as a function of concentration as in Fig. 7, and (iii) the average diffusivity from composite cell experiment in the literature, 5.0×10^{-10} cm^2/s. The overall stress level increases when smaller diffusion coefficients are used; the maximum stress with the measured diffusion coefficients [i.e., case (i) and (ii)] becomes more than ten times higher than the case of considerably higher diffusivity from the composite cathode measurement. When alternating diffusion coefficients are used in case (ii), the maximum stress reaches up to 70% of the minimum diffusion case in simulation (iii), although the overall diffusion value ranges 1 order of magnitude lower. The lower diffusion coefficients measured in this study, especially at the potential regions associated with peak currents, strongly affect the stress, resulting in the maximum von Mises stress of 110 MPa in this single particle simulation. It should be noted that our current model has not included the grain boundary modeling; so homogeneous analysis domain takes one single isotropic diffusion coefficient.

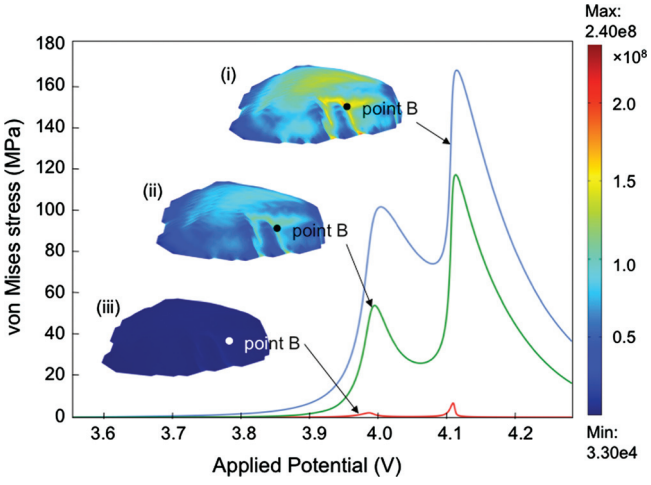

Figure 10. (Color online) von Mises stress generation with different diffusion coefficients, such as (i) the minimum of measured D_o, 3.0×10^{-12} cm^2/s, (ii) D_o as a function of concentration as in Fig. 7, and (iii) diffusivity from composite experiment in the literature, 5.0×10^{-10} cm^2/s.

Conclusions

Irregular but realistic particle surface geometry and diffusion coefficients were measured from dispersed single particles of $LiMn_2O_4$ cathode material. Dispersed cathode particle samples were suitable for investigating morphology of the particles using AFM. The 3D particle geometry was reconstructed from AFM scanning data. The single particle samples also showed a good cyclic behavior, and the diffusion coefficients were measured using both CV and PITT, ranging between 3.0×10^{-12} and 1.2×10^{-11} cm^2/s. The diffusivity values are close to the measurement from thin film experiments and 1–2 orders of magnitude lower than the values from composite cell experiments in the literature. This indicates the experiments with pure electrode materials, either in thin films or in particles, may lead to accurate diffusivity measurement without any parasitic effects from additives. Using thin film diffusivity data is also limited as they vary widely among the thin film fabrication techniques and processing conditions. The dispersed particle experiment was proposed as an alternative and suitable method of measuring diffusivities for the conventional particle-based Li-ion battery electrodes. Concentration dependent diffusion coefficients were implemented into single particle simulation with realistic particle geometry. The simulation results with concentration dependent diffusion coefficients showed that the $LiMn_2O_4$ particle could be under much higher intercalation-induced stress up to 110 MPa due to a slower diffusion around 4.01 and 4.13 V. Also, simulation with irregular particle shape showed that higher stress concentration could occur on sharply indented surface area of the particle.

Acknowledgment

This study is supported by the U.S. Department of Energy through the BATT program and by the General Motors Corporation. Support from our sponsors is gratefully acknowledged.

University of Michigan assisted in meeting the publication costs of this article.

References

1. X. C. Zhang, W. Shyy, and A. M. Sastry, *J. Electrochem. Soc.*, **154**, A910 (2007).
2. X. C. Zhang, A. M. Sastry, and W. Shyy, *J. Electrochem. Soc.*, **155**, A542 (2008).
3. J. Christensen and J. Newman, *J. Electrochem. Soc.*, **153**, A1019 (2006).
4. D. Guyomard and J. M. Tarascon, *J. Electrochem. Soc.*, **139**, 937 (1992).
5. H. Kanoh, Q. Feng, Y. Miyai, and K. Ooi, *J. Electrochem. Soc.*, **142**, 702 (1995).
6. Y. Xia, H. Takeshige, H. Noguchi, and M. Yoshio, *J. Power Sources*, **56**, 61 (1995).
7. D. A. Totir, B. D. Cahan, and D. A. Scherson, *Electrochim. Acta*, **45**, 161 (1999).
8. D. Zhang, B. N. Popov, and R. E. White, *J. Electrochem. Soc.*, **147**, 831 (2000).
9. K. A. Striebel, C. Z. Deng, S. J. Wen, and E. J. Cairns, *J. Electrochem. Soc.*, **143**, 1821 (1996).
10. M. Nishizawa, T. Uchiyama, K. Dokko, K. Yamada, T. Matsue, and I. Uchida, *Bull. Chem. Soc. Jpn.*, **71**, 2011 (1998).
11. D. Shu, K. Y. Chung, W. I. Cho, and K.-B. Kim, *J. Power Sources*, **114**, 253 (2003).

12. S. R. Das, S. B. Majumder, and R. S. Katiyar, *J. Power Sources*, **139**, 261 (2005).
13. S. B. Tang, M. O. Lai, and L. Lu, *Mater. Chem. Phys.*, **111**, 149 (2008).
14. K. Dokko, M. Nishizawa, M. Mohamedi, M. Umeda, I. Uchida, J. Akimoto, Y. Takahashi, Y. Gotoh, and S. Mizuta, *Electrochem. Solid-State Lett.*, **4**, A151 (2001).
15. K. Dokko, M. Mohamed, M. Umeda, and I. Uchida, *J. Electrochem. Soc.*, **150**, A425 (2003).
16. A. Clemencon, A. T. Appapillai, S. Kumar, and Y. Shao-Horn, *Electrochim. Acta*, **52**, 4572 (2007).
17. P. Delahay, *New Instrumental Methods in Electrochemistry*, p. 60, Interscience, New York (1954).
18. R. P. Frankenthal and I. Shain, *J. Am. Chem. Soc.*, **78**, 2969 (1956).
19. J. M. Tarascon, W. R. Mckinnon, F. Coowar, T. N. Bowmer, G. Amatucci, and D. Guyomard, *J. Electrochem. Soc.*, **141**, 1421 (1994).
20. I. Uchida, H. Fujiyoshi, and S. Waki, *J Power Sources*, **68**, 139 (1997).
21. C. J. Wen, B. A. Boukamp, R. A. Huggins, and W. Weppner, *J. Electrochem. Soc.*, **126**, 2258 (1979).
22. T. Nishina, H. Ura, and I. Uchida, *J. Electrochem. Soc.*, **144**, 1273 (1997).